A Vector Control Strategy to Eliminate Active Power Oscillations in Four-Leg Grid-Connected Converters Under Unbalanced Voltages

Andrés Mora, *Member, IEEE*, Roberto Cárdenas, *Senior Member, IEEE*, Matías Urrutia, *Student Member, IEEE*, Mauricio Espinoza, *Member, IEEE*, and Matías Díaz

***Abstract*— The problems associated with active power oscillations (APOs) in grid-connected converters are well-known. Imbalances in the grid usually produce double-frequency oscillations in the dc-link voltage and current which could reduce the useful life of solar panels, batteries, and capacitors connected to this point. Moreover, as reported in the literature, double-frequency reactive power oscillations (RPOs) also produce adverse effects in distribution systems, and it is desirable to eliminate or mitigate them. When a four-leg power converter is connected to an unbalanced grid, the zero-sequence current provides extra degrees of freedom to compensate or even eliminate the power oscillations at the converter dc-link side. In this paper, a new methodology to regulate these double-frequency power components is proposed. It is based on a closed-loop vector control approach, where the active power oscillations (APOs) at converter side are transformed into a synchronous frame rotating at twice the grid frequency and regulated using the zero-sequence current. To avoid overcurrent produced by the circulation of positive-, negative-, and zero-sequence components a current limiter is also proposed in this paper. Experimental results obtained with a 4-kW four-leg power converter prototype are presented and discussed in this paper.**

***Index Terms*— DC–AC converters, distribution system, power control, symmetrical components.**

I. Introduction

In the past few years, the integration of energy resources into distributed systems (DSs) and microgrids (MGs) has emerged as a critical issue driven by environmental motivations and economic incentives [1]. A typical MG could be composed of a cluster of loads, distributed generators, and energy storage systems connected to the main ac power system at the distribution level [2], [3]. Low-voltage MGs and DSs are typically unbalanced electrical networks [4], [5] considering the untransposed structure of their distribution lines, the integration of distributed resources (DRs), and the presence of both single- and two-phase loads. Typical electrical network structures for low-voltage DSs are: 1) three-phase three-wire (3P3W) and 2) three-phase four-wire (3P4W) systems.

In 3P4W systems, a path for circulation of zero-sequence current is required to interface distributed generation units. This fourth wire can be provided by a bulky delta-star transformer (where the neutral point of secondary is used) which have usually very low power to weight and power to volume ratios, or by a split-capacitor power converter (using the midpoint of the dc-link). However, these methods usually reduce the utilization of the dc-link voltage or produce high-ripple in the dc-link capacitors [6]. Moreover, when power transformers are used, there is reduced controllability of the zero-sequence signals applied to the grid/load. Therefore, the four-leg power converters are probably the best solution to provide this fourth wire, providing full utilization of the dc-link voltage, and control over the zero-sequence components [7]. Note that the four-leg voltage source converters (VSCs) converters can be utilized in many applications. For instance, for collaborative power-sharing control of the active and reactive powers of the loads connected to a MG [8]–[10]; fault ride through control [10]; fault current limitation [9]; active power filtering [11]; interfacing of energy storage systems to the MG [12]. In case galvanic isolation is required, a star/star transformer could be used to provide isolation maintaining the control of the zero-sequence component.

Because of the inherent network imbalances in four-leg MGs, APOs and RPOs may flow between loads and power converters. In the case of VSCs, APO may lead to large fluctuations of the dc-link voltage and current. This oscillation phenomenon could cause problems such as over-voltage, output distortion, or even instability [13]. Moreover, in wind and solar energy conversion systems, fuel cells and batteries [12], large ripple currents and ripple voltages could considerably reduce the efficiency, lifetime, and long-term reliability of dc-link capacitors, PVs and energy storage systems [14]–[17]. Furthermore, RPO can produce a current operating rise,

Manuscript received January 17, 2019; revised March 29, 2019 and May 30, 2019; accepted June 2, 2019. Date of publication June 6, 2019; date of current version May 6, 2020. This work was supported in part by Fondecyt Chile under Grant 1180879 and in part by the Basal Project FB0008 "Advanced Center for Electrical and Electronic Engineering." The work of A. Mora was supported by the Conicyt Grant CONICYT-PCHA/Doctorado Nacional/2013-21130042. Recommended for publication by Associate Editor Xinbo Ruan. *(Corresponding author: Andrés Mora.)*

A. Mora and M. Urrutia are with the Department of Electrical Engineering, Universidad Técnica Federico Santa María, Valparaíso 8370071, Chile (e-mail: a.mora@ieee.org; matias.urrutia@usm.cl).

R. Cárdenas is with the Department of Electrical Engineering, Universidad de Chile, Santiago 8370451, Chile (e-mail: rcd@ieee.org; feldonoso@ing.uchile.cl).

M. Espinoza is with the School of Electrical Engineering, Universidad de Costa Rica, San Pedro 11501-2060, Costa Rica (e-mail: maeb@ieee.org).

M. Díaz is with the Department of Electrical Engineering, Universidad de Santiago de Chile, Santiago 9170124, Chile (e-mail: matias.diazd@usach.cl).

Color versions of one or more of the figures in this article are available online at http://ieeexplore.ieee.org.

Digital Object Identifier 10.1109/JESTPE.2019.2921536

contribute to increase the power losses, and negatively impact the point of common coupling (PCC) voltage [18], [19].

For the reasons mentioned above, it is attractive and advantageous to suppress the APO and RPO. However, this selection is not straightforward and depends on practical requirements. In 3P3W power converters, it is not possible to regulate both without introducing harmonic distortion in the output currents [20], [21]. Several methods have been proposed to enhance the performance of three-leg power converters under unbalance grid voltages, looking to either balance the three-phase ac currents or to minimize the APO-RPO, depending on the control objectives desired [20]–[25].

In this context, the degrees of freedom provided by the three-leg power converter are not always sufficient to compensate power oscillations and more degrees of freedom are required to improve the operation of grid-connected VSCs under unbalanced ac source conditions. These additional degrees of freedom can be provided by the amplitude and angular phases of the zero-sequence current in the additional path introduced by the fourth wire of the four-leg VSC [13], [26]. In [13], this current is computed to eliminate APO and RPO at the PCC while the dc components of the active/reactive powers are tracking the provided reference values. However, the algorithm proposed in [13] assumes that the phase of the zero-sequence voltage is in phase with the grid voltage of phase a and this is certainly an oversimplification which is valid in some operating points only. Therefore, it is not a generalized solution which can be applied to any grid-operating condition. Moreover, the control systems discussed previously are open-loop algorithms that do not have the same performance than that obtained with closed-loop systems and the control aims in [13] are not the eliminations of the APO at the converter side, where the dc-link capacitors are located.

In this paper, a new control system for four-leg converters in MG applications is discussed. A closed-loop control strategy that directly regulates the power oscillations is implemented, and the extra degrees of freedom provided by the zero-sequence signals are used. The contributions of this paper can be summarized as follows.

1) This paper presents a closed-loop control strategy for canceling/mitigating the APO at the converter side and, thus, in the dc-link electrical variables. The control system utilizes the two additional degrees of freedom provided by the fourth leg of the power converter and in some operating points could cancel both the APO in the converter side as well as the RPO at the grid side.
2) A vector representation of the APO is presented in this paper. This modeling allows the use of vector control techniques to eliminate/mitigate the power oscillations. Therefore, simple controllers implemented in the synchronous rotating frame can be used to regulate with zero steady-state tracking error the double-frequency oscillations in the dc-link electrical variables using currents of positive-, negative-, and zero-sequence.
3) A simple algorithm to avoid overcurrent in the converter legs is proposed. The control system also allows selecting if only part of the APO and/or RPO is compensated.

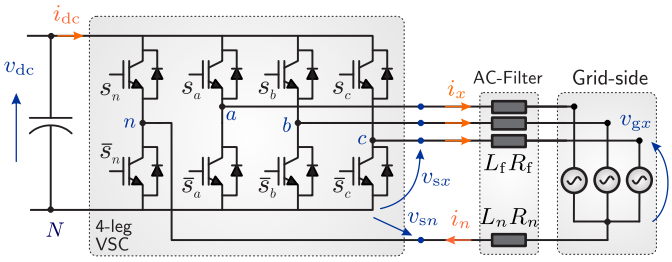

Fig. 1. Grid-connected four-leg two-level VSC converter.

The rest of this paper is organized as follows. In Section II, the modeling of the four-leg VSC and grid system is discussed. In Section III, the proposed control strategies are introduced and extensively analyzed. In Section IV, the experimental results obtained with a 4-kW prototype are presented. Finally, an appraisal of the proposed methodology is discussed in the conclusions.

II. Modeling of VSC-Grid Systems

A. Fundamental Relations

To formulate the control strategy, the instantaneous electrical variables of the grid and the converter are defined in terms of their respective currents and voltages with a convenient usage of the $\alpha\beta 0$ transform [27]. This transformation maps the instantaneous three-phase variables ξ_{abc} into instantaneous decoupled variables on the $\alpha\beta 0$-axis according to

$$\begin{bmatrix} \xi_\alpha \\ \xi_\beta \\ \xi_0 \end{bmatrix} = \sqrt{\frac{2}{3}} \begin{bmatrix} 1 & -\frac{1}{2} & -\frac{1}{2} \\ 0 & \frac{\sqrt{3}}{2} & -\frac{\sqrt{3}}{2} \\ \frac{1}{\sqrt{2}} & \frac{1}{\sqrt{2}} & \frac{1}{\sqrt{2}} \end{bmatrix} \begin{bmatrix} \xi_a \\ \xi_b \\ \xi_c \end{bmatrix}. \tag{1}$$

From the grid side of the system shown in Fig. 1, the voltages and currents are, respectively, specified as

$$\boldsymbol{v}_g = v_\alpha + jv_\beta, \quad \boldsymbol{i}_g = i_\alpha + ji_\beta. \tag{2}$$

Using (1) and (2), the instantaneous complex power expression for the grid side can be described by [27]

$$\boldsymbol{s}_g = \boldsymbol{v}_g \boldsymbol{i}_g^* + v_0 i_0 \tag{3}$$

where i_0 and v_0 are, respectively, the zero-sequence current and the zero-sequence grid voltage obtained from (1); additionally, $\boldsymbol{i}_g^*$ refers to the complex conjugate of $\boldsymbol{i}_g$. In addition, on the converter-side illustrated in Fig. 1, the instantaneous power is defined as

$$p_s = v_{sa} i_a + v_{sb} i_b + v_{sc} i_c - i_n v_{sn} \tag{4}$$

where $i_n = (3i_0)^{1/2}$ is the neutral current, and v_{sx} is the output converter voltage in the leg x ($x \in \{a, b, c, n\}$) measured from the negative point N of the dc-link (shown in Fig. 1. Thus, using (1) in (4), the instantaneous power injected by the converter is

$$p_s = \Re\{\boldsymbol{v}_s \boldsymbol{i}_g^*\} + v_{s0} i_0 \tag{5}$$

where $\boldsymbol{v}_{\rm s}$ and $v_{\rm s0}$ are, respectively, the converter voltage vector and the common-mode voltage of the converter defined as

$$v_{\rm s0} = \frac{1}{\sqrt{3}}(v_{sa} + v_{sb} + v_{sc}) - \sqrt{3}v_{sn}. \tag{6}$$

Moreover, if the voltage equilibrium equation

$$\boldsymbol{v}_{\rm s} = L_{\rm f}\frac{{\rm d}\boldsymbol{i}_{\rm g}}{{\rm d}t} + R_{\rm f}\boldsymbol{i}_{\rm g} + \boldsymbol{v}_{\rm g} \tag{7}$$

is replaced into (5), the active power delivered by the four-leg VSC becomes

$$p_{\rm s} = \Re\left\{\boldsymbol{v}_{\rm g}\boldsymbol{i}_{\rm g}^*\right\} + R_{\rm f}|\boldsymbol{i}_{\rm g}|^2 + L_{\rm f}\Re\left\{\frac{{\rm d}\boldsymbol{i}_{\rm g}}{{\rm d}t}\boldsymbol{i}_{\rm g}^*\right\} + v_{\rm s0}i_0. \tag{8}$$

Therefore, as shown in (8), the active power of the converter is composed of the grid power, the power consumed by the three-phase filter, and the zero-sequence power on the converter-side $p_{\rm s0} = v_{\rm s0}i_0$. Consequently, if imbalances are presented on the grid voltages, $p_{\rm s0}$ can be used to mitigate the double-frequency oscillations in the active power of the converter-side $p_{\rm s}$. Note that from (3), the oscillations in the reactive power cannot be compensated using $p_{\rm g0} = v_0 i_0$, because the zero-sequence components cannot produce instantaneous reactive power (see [27]). Hence, the RPO should be mitigated using a suitable negative-sequence current in the grid current vector $\boldsymbol{i}_{\rm g}$.

Similarly, the common-mode voltage equilibrium law for the VSC-grid system is given by

$$v_{\rm s0} = L_0\frac{{\rm d}i_0}{{\rm d}t} + R_0 i_0 + v_0 \tag{9}$$

being $L_0 = L_{\rm f} + 3L_n$ and $R_0 = R_{\rm f} + 3L_n$, the zero-sequence inductance and resistance, respectively. Thus, the zero-sequence power on the converter-side is described by

$$p_{\rm s0} = L_0\ i_0\frac{{\rm d}i_0}{{\rm d}t} + R_0 i_0^2 + v_0 i_0. \tag{10}$$

It is worth to highlight here that the previous relationships are stated both for 3P3W and 3P4W systems. In the case of analyzing a 3P3W configuration, then the zero-sequence current is established as zero, i.e., $i_0 = 0$.

B. Modeling of 3P3W Systems

The methodology to eliminate the APO in 3P3W systems has already been discussed in the previous publications, e.g., [20]. However, for completeness, it is briefly presented in this section.

Restricting the analysis to the fundamental grid-frequency ω, the voltage and current vectors of a 3P3W system can be conveniently described by the instantaneous symmetrical sequence components as [28], [29]

$$\boldsymbol{v}_{\rm g} = \boldsymbol{v}_1\,{\rm e}^{j\omega t} + \boldsymbol{v}_2\,{\rm e}^{-j\omega t} = \boldsymbol{v}_{1\alpha\beta} + \boldsymbol{v}_{2\alpha\beta} \tag{11}$$

$$\boldsymbol{i}_{\rm g} = \boldsymbol{i}_1\,{\rm e}^{j\omega t} + \boldsymbol{i}_2\,{\rm e}^{-j\omega t} = \boldsymbol{i}_{1\alpha\beta} + \boldsymbol{i}_{2\alpha\beta} \tag{12}$$

where $\boldsymbol{v}_{1\alpha\beta}$ and $\boldsymbol{v}_{2\alpha\beta}$ are, respectively, the positive- and negative-sequence components of the grid voltage vector in the $\alpha\beta$ frame that can be expressed in the positive- and negative- synchronous reference frame (SRF), respectively, as $\boldsymbol{v}_1 = v_{1d} + jv_{1q}$, and $\boldsymbol{v}_2 = v_{2d} + jv_{2q}$. Similarly, the grid current vector can also be expressed in terms of $\boldsymbol{i}_1$ and $\boldsymbol{i}_2$, as shown in (12). Thereby, from (3), the instantaneous complex power expression of the grid side can be expressed as

$$\boldsymbol{s}_{\rm g12} = \underbrace{\boldsymbol{v}_1\boldsymbol{i}_1^* + \boldsymbol{v}_2\boldsymbol{i}_2^*}_{\overline{\boldsymbol{s}}_{g12}} + \underbrace{\boldsymbol{v}_1\boldsymbol{i}_2^*\,{\rm e}^{j2\omega t} + \boldsymbol{v}_2\boldsymbol{i}_1^*\,{\rm e}^{-j2\omega t}}_{\widetilde{\boldsymbol{s}}_{g12}} \tag{13}$$

where $\overline{\boldsymbol{s}}_{\rm g12}$ groups the active and reactive average powers, and $\widetilde{\boldsymbol{s}}_{\rm g12}$ groups the oscillating components fluctuating at twice the fundamental grid frequency. Consequently, the oscillating active and reactive powers are defined by

$$\widetilde{p}_{\rm g12} = \Re\{\widetilde{\boldsymbol{s}}_{\rm g12}\} = \Re\left\{\left(\boldsymbol{v}_1^*\boldsymbol{i}_2 + \boldsymbol{v}_2\boldsymbol{i}_1^*\right){\rm e}^{-j2\omega t}\right\} \tag{14}$$

$$\widetilde{q}_{\rm g12} = \Im\{\widetilde{\boldsymbol{s}}_{\rm g12}\} = \Im\left\{\left(\boldsymbol{v}_2\boldsymbol{i}_1^* - \boldsymbol{v}_1^*\boldsymbol{i}_2\right){\rm e}^{-j2\omega t}\right\}. \tag{15}$$

The negative-sequence current $\boldsymbol{i}_2$ represents one of the degrees of freedom to mitigate the power oscillations. This component allows manipulating both APO and RPO shown in (14) and (15), respectively. In this regard, using the following negative-sequence current:

$$\boldsymbol{i}_2^{\rm ref} = \mu\frac{\boldsymbol{v}_2\boldsymbol{v}_1}{|\boldsymbol{v}_1|^2}\boldsymbol{i}_1^* \tag{16}$$

both oscillating power components can be written as

$$\widetilde{p}_{\rm g12} = (1+\mu)\Re\left\{\boldsymbol{v}_2\boldsymbol{i}_1^*\,{\rm e}^{-j2\omega t}\right\} \tag{17}$$

$$\widetilde{q}_{\rm g12} = (1-\mu)\Im\left\{\boldsymbol{v}_2\boldsymbol{i}_1^*\,{\rm e}^{-j2\omega t}\right\}. \tag{18}$$

Thus, the amplitudes of $\widetilde{p}_{\rm g12}$ and $\widetilde{q}_{\rm g12}$ vary as a function of the scalar parameter $\mu\in[-1,\ 1]$ according to

$$\Delta P_{g12} = (1+\mu)\left|\boldsymbol{v}_2\boldsymbol{i}_1^*\right| \tag{19}$$

$$\Delta Q_{g12} = (1-\mu)\left|\boldsymbol{v}_2\boldsymbol{i}_1^*\right|. \tag{20}$$

In addition, by replacing (16) into (13), and assuming a SRF oriented along the positive-sequence grid voltage, i.e., $\boldsymbol{v}_1 = v_{1d}$, the positive-sequence current reference $\boldsymbol{i}_1^{\rm ref}$ can be expressed in terms of the required active and reactive power references ($P_{\rm g}^{\rm ref}$ and $Q_{\rm g}^{\rm ref}$, respectively), as follows:

$$\boldsymbol{i}_1^{\rm ref} = \lambda_d P_{\rm g}^{\rm ref} + j\lambda_q Q_{\rm g}^{\rm ref} \tag{21}$$

where

$$\lambda_d = \frac{|\boldsymbol{v}_1|}{|\boldsymbol{v}_1|^2 + \mu|\boldsymbol{v}_2|^2};\quad \lambda_q = \frac{|\boldsymbol{v}_1|}{\mu|\boldsymbol{v}_2|^2 - |\boldsymbol{v}_1|^2} \tag{22}$$

are the scalars that are the function of the amplitude of $\boldsymbol{v}_1$ and $\boldsymbol{v}_2$ and the parameter μ.

Therefore, when the grid current vector $\boldsymbol{i}_{\rm g}$ is regulated using the positive- and negative-sequence currents given by (16) and (21), the active and reactive powers track their required average values; however, simultaneously a tradeoff between the amplitude of their oscillating components is established by tuning the parameter μ. For instance, if negative-sequence currents are not allowed, then this parameter can be defined as $\mu = 0$; and consequently, both the instantaneous active/reactive powers are affected by double-frequency oscillations under unbalanced grid conditions.

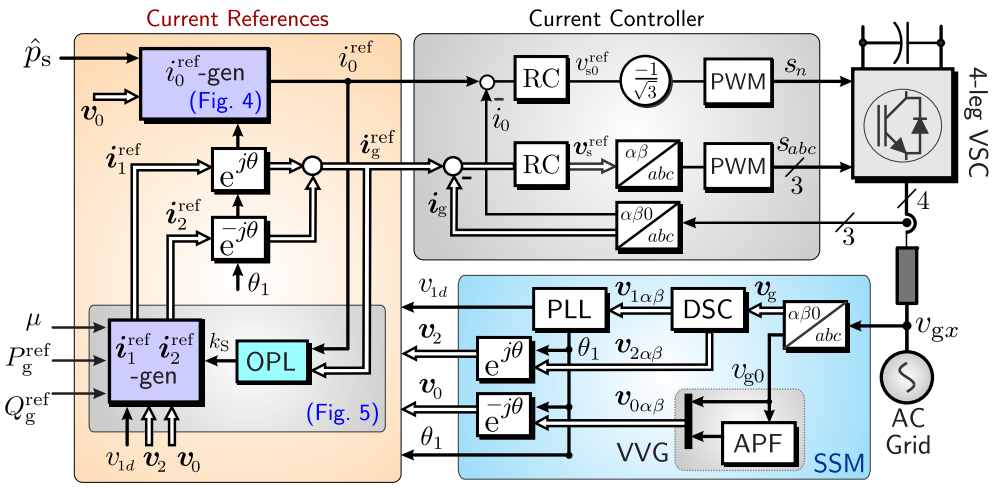

Fig. 2. Proposed control structure for the grid-connected four-leg VSC.

III. Proposed Control Strategy to Eliminate the APO in 3P4W Topologies

As mentioned earlier, in 3P3W systems, there are not sufficiently degrees of freedom to eliminate both the APO and RPO by supplying undistorted currents to the grid [20], [21], [30], [31]. To overcome this limitation, the current circulating through the fourth wire of the four-leg VSC, $i_n = \sqrt{3}i_0$, can be used to obtain the two additional degrees of freedom required to eliminate/mitigate the APO at the converter- or grid-side [13], [26].

The nested control scheme depicted in Fig. 2 is proposed in this work to control the grid-connected 4-leg VSC. This strategy allows removing the APO at the converter-side as well as at the grid-side by properly computing the zero-sequence current reference i_0^{ref}. Note that the methodology to calculate i_0^{ref} is introduced in Fig. 4 and it is extensively discussed in Sections III-A and III-B.

As shown in Fig. 2, the outer loop is focused on computing the grid current references $\boldsymbol{i}_g^{ref}$ and i_0^{ref} utilizing the instantaneous symmetrical components $\boldsymbol{i}_{120}^{ref} = [\boldsymbol{i}_1^{ref}\ \boldsymbol{i}_2^{ref}\ i_0^{ref}]$ that allows eliminating/mitigating the APO at the converter- or grid-side. As depicted in the gray block of Fig. 2, the resulting grid current vector and the zero-sequence current references are controlled in the $\alpha\beta 0$ frame using PR controllers, providing zero steady-state error for both the grid current vector $\boldsymbol{i}_g$ and the zero-sequence current i_0.

In addition, as shown in the orange block of Fig. 2, the instantaneous symmetrical sequence components $\boldsymbol{i}_1^{ref}$ and $\boldsymbol{i}_2^{ref}$ are computed from the active/reactive power references, the parameter μ, and also from the instantaneous sequence components of the grid voltage oriented along its positive-sequence (i.e., v_{1d}, $\boldsymbol{v}_0$, and $\boldsymbol{v}_2$). These sequence components are obtained by employing the sequence separation method (SSM) shown in the light-blue area of Fig. 2. On this subject, the positive- and negative-sequence components are obtained by using the standard delay signal cancellation (DSC) method [32], [33], and the zero-sequence component is computed by using a virtual vector generator (VVG) based on an orthogonal signal generator (OSG). An output power limiter (OPL) is introduced to operate the converter inside its rated current capability by adjusting the scalar k_S. More details regarding this block are introduced in Section III-D.

Although several OSG techniques have been proposed in [19], in this work, an all-pass filter (APF) [34] is preferred due to implementation simplicity and good performance for small variations in the MG electrical frequency. For completeness, a brief discussion is realized in the following.

The APF transfer function is

$$G_{APF}(s) = \frac{\omega - s}{\omega + s}. \tag{23}$$

It is assumed that the zero-sequence voltage signal is $v_{g0} = V_0 \cos \omega t$, which according to the VVG principle is defined as $v_{0\alpha}$. Using the Laplace transform of $v_{0\alpha}$ and (23), the virtual component $v_{0\beta}$ is obtained as

$$v_{0\beta}(s) = \frac{sV_0}{(s^2+\omega^2)}\frac{(\omega - s)}{(\omega + s)} = V_0\left(\frac{\omega}{s^2+\omega^2} - \frac{1}{s+\omega}\right). \tag{24}$$

Then, by using the inverse Laplace transform for $v_{0\beta}(s)$, the virtual voltage vector is given by

$$\boldsymbol{v}_{0\alpha\beta} = V_0 \cos \omega t + j\, V_0(\sin \omega t - e^{-\omega t}). \tag{25}$$

Therefore, for the VVG shown in Fig. 2, under any change or perturbation of the zero-sequence grid voltage, the estimation of its corresponding virtual vector is affected by the transient of the term $e^{-\omega t}$ of (25) which in a 50-Hz grid will be negligible after about 15 ms. This delay is higher than that produced typically by the DSC and has to be taken into account when control systems relying on the OSG are considered.

A. Converter-Side APO Elimination

The zero-sequence variables v_0 and i_0 can be conveniently written using the vector notation as

$$v_0 = \frac{1}{2}(\boldsymbol{v}_0\, e^{j\omega t} + \boldsymbol{v}_0^*\, e^{-j\omega t}) = \frac{1}{2}(\boldsymbol{v}_{0\alpha\beta} + \boldsymbol{v}_{0\alpha\beta}^*) \tag{26}$$

$$i_0 = \frac{1}{2}(\boldsymbol{i}_0\, e^{j\omega t} + \boldsymbol{i}_0^*\, e^{-j\omega t}) = \frac{1}{2}(\boldsymbol{i}_{0\alpha\beta} + \boldsymbol{i}_{0\alpha\beta}^*) \tag{27}$$

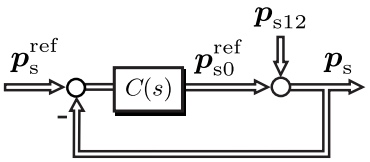

Fig. 3. Closed-loop control for OPV control.

with $\boldsymbol{v}_{0\alpha\beta}$ and $\boldsymbol{i}_{0\alpha\beta}$ the virtual vectors of the zero-sequence voltage and current, respectively. Notie that these virtual vectors can also be expressed in a particular SRF as $\boldsymbol{v}_0 = v_{0d} + jv_{0q}$ and $\boldsymbol{i}_0 = i_{0d} + ji_{0q}$, respectively.

It is straightforward to prove that using (26) and (27), both the average component and oscillating component of $p_{\rm s0}$ [see (10)] are, respectively, given by

$$\overline{p}_{\rm s0} = \frac{1}{2}R_0|\boldsymbol{i}_0|^2 + \frac{1}{2}\Re\{\boldsymbol{v}_0\boldsymbol{i}_0^*\} \tag{28}$$

$$\widetilde{p}_{\rm s0} = \frac{1}{2}\Re\{(\boldsymbol{Z}_0\boldsymbol{i}_0\boldsymbol{i}_0 + \boldsymbol{v}_0\boldsymbol{i}_0)\,{\rm e}^{j2\omega t}\} \tag{29}$$

with $\boldsymbol{Z}_0 = R_0 + j\omega L_0$, the zero-sequence impedance at the fundamental frequency.

On the other hand, from (8), the APO at the converter-side can be decomposed as

$$\widetilde{p}_{\rm s} = \widetilde{p}_{\rm s12} + \widetilde{p}_{\rm s0} \tag{30}$$

where $\widetilde{p}_{\rm s12}$ is the APO produced by the positive- and negative-sequence components of the grid voltage and current. It follows that, by replacing (11) and (12) into (8), $\widetilde{p}_{\rm s12}$ can be expressed as

$$\widetilde{p}_{\rm s12} = \Re\left\{\left(\boldsymbol{v}_1\boldsymbol{i}_2^* + \boldsymbol{v}_2^*\boldsymbol{i}_1 + 2\boldsymbol{Z}_{\rm f}\boldsymbol{i}_1\boldsymbol{i}_2^*\right){\rm e}^{j2\omega t}\right\} \tag{31}$$

with $\boldsymbol{Z}_{\rm f} = R_{\rm f} + j\omega L_{\rm f}$, the impedance of the three-phase filter. Therefore, to eliminate the APO at the converter side, as derived from (30), the challenge is to obtain a zero-sequence current such that

$$\widetilde{p}_{\rm s0} = -\widetilde{p}_{\rm s12}. \tag{32}$$

In this regard, if $\boldsymbol{i}_2$ is regulated for tracking the reference given in (16), the required additional sequence components $\boldsymbol{i}_0$ and $\boldsymbol{i}_1$, which allow either satisfy (32) [using (29) and (31)] and inject the desired active and reactive power references, can be found by solving the following system of nonlinear complex equations :

$$\boldsymbol{Z}_0\boldsymbol{i}_0^2 + \boldsymbol{v}_0\boldsymbol{i}_0 = -2(1+\mu)\boldsymbol{v}_2^*\boldsymbol{i}_1 - 4\mu\boldsymbol{Z}_{\rm f}\frac{\boldsymbol{v}_1^*\boldsymbol{v}_2^*}{|\boldsymbol{v}_1|^2}\boldsymbol{i}_1^2 \tag{33a}$$

$$\boldsymbol{i}_1 = \lambda_d\left(P_{\rm g}^{\rm ref} - \frac{1}{2}\Re\{\boldsymbol{v}_0\boldsymbol{i}_0^*\}\right) + j\lambda_q Q_{\rm g}^{\rm ref}. \tag{33b}$$

However, to solve (33) in real time could pose a relatively high computational burden. In addition, it is susceptible to parameters mismatch. To avoid this costly implementation and parameter uncertainty, an alternative closed-loop power vector-based approach is introduced in this work.

Without loss of generality, the oscillating component of the active power at the converter side can be expressed as follows:

$$\widetilde{p}_{\rm s} = \frac{1}{2}\boldsymbol{p}_{\rm s}\,{\rm e}^{j2\omega t} + \frac{1}{2}\boldsymbol{p}_{\rm s}^*\,{\rm e}^{-j2\omega t}. \tag{34}$$

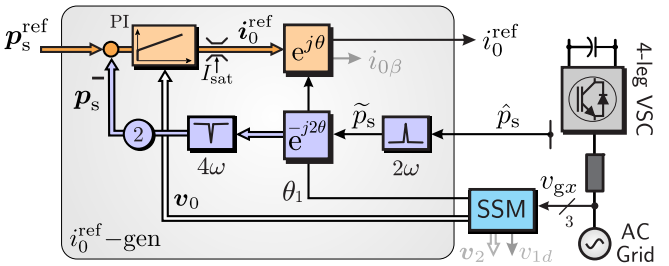

Fig. 4. Zero-sequence generator for converter-side APO Elimination.

Referring (34) to a SRF rotating at 2ω, the following dq representation of $\widetilde{p}_{\rm s}$ can be obtained:

$$\widetilde{p}_{{\rm s}dq} = \frac{1}{2}\boldsymbol{p}_{\rm s} + \frac{1}{2}\boldsymbol{p}_{\rm s}^*{\rm e}^{-4\omega t}. \tag{35}$$

Hence, from (30) and by only focusing on the dc-component in the right-hand side of (35) (the other component is filtered out by the 4ω notch filter shown in Fig. 4), the converter-side oscillating power vector (OPV) $\boldsymbol{p}_{\rm s}$ can be defined as

$$\boldsymbol{p}_{\rm s} = \boldsymbol{p}_{\rm s0} + \boldsymbol{p}_{\rm s12}. \tag{36}$$

Therefore, a closed-loop control based on a PI controller that utilizes the zero-sequence OPV $\boldsymbol{p}_{\rm s0}$ as the control action can be implemented to regulate $\boldsymbol{p}_{\rm s}$ to the desired reference value $\boldsymbol{p}_{\rm s}^{\rm ref} = 0$, as illustrated in the simplified control diagram shown in Fig. 3. Thereby, if the PI controller is expressed in the s-domain as $C(s)$, the resulting closed-loop transfer function for $\boldsymbol{p}_{\rm s}(s)$ is given by

$$\boldsymbol{p}_{\rm s}(s) = \frac{C(s)}{1+C(s)}\boldsymbol{p}_s^{\rm ref} + \frac{1}{1+C(s)}\boldsymbol{p}_{\rm s12}. \tag{37}$$

From (37), it is concluded that the oscillating power produced by the positive- and negative-sequence components (represented by the OPV $\boldsymbol{p}_{\rm s12}$) can be modeled as a disturbance in a closed-loop fashion. Thus, it is compensated due to the integral action of the controller. Nevertheless, according to (29), the zero-sequence current that produces the desired zero-sequence OPV $\boldsymbol{p}_{\rm s0}^{\rm ref}$ has to fullfil the following nonlinear relation:

$$\boldsymbol{p}_{\rm s0}^{\rm ref} = \frac{1}{2}\boldsymbol{v}_0\boldsymbol{i}_0 + \frac{1}{2}\boldsymbol{Z}_0\boldsymbol{i}_0^2. \tag{38}$$

Consequently, this paper proposes to directly use the zero-sequence current vector $\boldsymbol{i}_0$ as the PI controller outputs which also allows limiting the amplitude of the zero-sequence current to be injected by the four-leg power converter.

B. Generation of the Zero-Sequence Current Reference

The closed-loop zero-sequence current reference generator, shown in Fig. 4, is proposed in this paper to eliminate the APOs in the converter side; and thus, in the dc-link electrical variables. To accomplish the control target, this controller compares the converter-side OPV $\boldsymbol{p}_{\rm s}$ with its reference $\boldsymbol{p}_{\rm s}^{\rm ref} = 0$ and utilizes the zero-sequence current vector reference $\boldsymbol{i}_0^{\rm ref}$ as the control action. Then, the required instantaneous

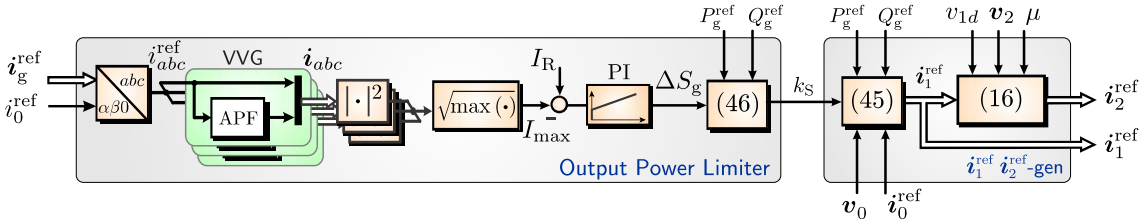

Fig. 5. Signal flow of the OPL and the positive- and negative-sequence current references.

zero-sequence current is finally computed by evaluating (27) with $\boldsymbol{i}_0^{\text{ref}} = i_{0d}^{\text{ref}} + j i_{0q}^{\text{ref}}$ as

$$i_0^{\text{ref}} = i_{0d}^{\text{ref}} \cos\theta_1 - i_{0q}^{\text{ref}} \sin\theta_1 \tag{39}$$

where θ_1 is the angular position of the positive-sequence voltage vector. Note that (39) is equivalent to take the real part of the vector $\boldsymbol{i}_0^{\text{ref}}$ referred to the stationary frame, as illustrated in Fig. 4 with the operator $e^{j\theta_1}$.

In the proposed closed-loop zero-sequence current generator shown in Fig. 4, the converter-side APO $\boldsymbol{p}_s$ is derived from the instantaneous active power injected by the converter p_s. This active power can be estimated from (5) using the measured grid currents and the outputs of the inner current controllers as follows:

$$\hat{p}_s = \Re\{\boldsymbol{v}_s^{\text{ref}} \boldsymbol{i}_g^*\} + v_{s0}^{\text{ref}} i_0. \tag{40}$$

As depicted in the purple blocks of Fig. 4, this estimation is filtered by using a passband filter tuned at twice of the grid frequency. According to (36), an additional notch filter centered at 4ω is required to finally obtain the converter-side OPV in dq coordinates, $\boldsymbol{p}_s$.

C. Small Signal Model for the Tuning of the PI Controller

Assuming that the control loop that regulates the APOs is designed with a relatively slow dynamic performance, then the plant required to tune the controllers can be represented by the gains obtained from a small signal model. In this regard, the linearized model is directly obtained from (38) as follows:

$$\frac{\Delta \boldsymbol{p}_{s0}}{\Delta \boldsymbol{i}_0} = \boldsymbol{K}_0 = \frac{1}{2}\boldsymbol{v}_0 + \boldsymbol{Z}_0 \boldsymbol{I}_0 \tag{41}$$

with $\boldsymbol{I}_0$ the equilibrium zero-sequence current. Hence, the above equation allows defining the relation between both power and current vectors as a proportional plant with a complex gain $\boldsymbol{K}_0$. Thereby, if (41) is decomposed in its dq components, the following coupled system is derived:

$$\Delta p_{s0d} = K_{0d}\Delta i_{0d} - K_{0q}\Delta i_{0q} \tag{42}$$

$$\Delta p_{s0q} = K_{0d}\Delta i_{0q} + K_{0q}\Delta i_{0d} \tag{43}$$

Hence, both components have the same gain K_{0d} and the term of cross-coupling is determined by the gain K_{0q}. By inspecting (41), it is simple to conclude that the gains K_{0d} and K_{0q} are strongly dependent on the zero-sequence voltage vector $\boldsymbol{v}_0$. Therefore, to simplify the controller design, the cross-coupling terms, dominated by the gain K_{0q}, are considered as disturbances. Accordingly, as shown in Fig. 4, the d-component of $\boldsymbol{v}_0$ is used by the PI controller to adjust its gain which allows maintaining the control system operating stably with a good dynamic response in the whole operating range.

D. Converter Output Current Limiter

As discussed in the previous sections, the proposed control diagrams shown in Figs. 2 and 4 are used to eliminate/mitigate the APO and RPO at the converter side. However, because the instantaneous currents are derived from the symmetrical components $\boldsymbol{i}_{120}$, a suitable current limiter has to be implemented to avoid operating outside the nominal values in any of the converter legs.

The proposed current limiter has two stages. First, the neutral current i_n is directly limited by using a conventional anti-windup strategy for the PI controller that produces $\boldsymbol{i}_0^{\text{ref}}$, as shown the control diagram in Fig. 4. Hence, the current of the fourth wire is limited to the maximum amplitude $I_{\text{sat}} \leq I_R/\sqrt{3}$, with I_R being the peak value of the converter nominal current.

Second, to fulfill with the thermal constraint of the other three phases of the four-leg converter shown in Fig. 1, an additional control stage, depicted in Fig. 5, is included into the overall control scheme of Fig. 2. This additional stage is called OPL, and it is designed to reduce the apparent power supplied to the grid in order to drive the converter inside its rated capability by manipulating the positive-sequence current reference.

As shown in Fig. 5, the algorithm stars using i_0^{ref} and the initial current vector reference $\boldsymbol{i}_g^{\text{ref}}$. Then, the desired abc grid currents $i_{\text{abc}}^{\text{ref}}$ are computed by employing the inverse $\alpha\beta 0$ transformation given in (1). The maximum peak value of these currents $I_{\max}$ is computed using their corresponding virtual current vectors $\boldsymbol{i}_x = i_{x\alpha} + j i_{x\beta}$ with $x \in \{a, b, c\}$ (derived from the VVG blocks shown in green color in Fig. 5) as follows:

$$I_{\max} = \sqrt{\max\left(i_{a\alpha}^2 + i_{a\beta}^2,\ i_{b\alpha}^2 + i_{b\beta}^2,\ i_{c\alpha}^2 + i_{c\beta}^2\right)}. \tag{44}$$

As depicted in Fig. 5, $I_{\max}$ is compared with the peak value of the converter nominal current I_R to generate the input error of a PI regulator. This controller acts over the apparent power reference reducing its value in $\Delta S_g \leq 0$. Therefore, the positive-sequence current reference is updated using (33b) according to

$$\boldsymbol{i}_1^{\text{ref}} = \lambda_d \left(\left(k_s P_g^{\text{ref}}\right) - \frac{1}{2}\Re\{\boldsymbol{v}_0^* \boldsymbol{i}_0^{\text{ref}}\} \right) + j\lambda_q \left(k_s Q_g^{\text{ref}}\right) \tag{45}$$

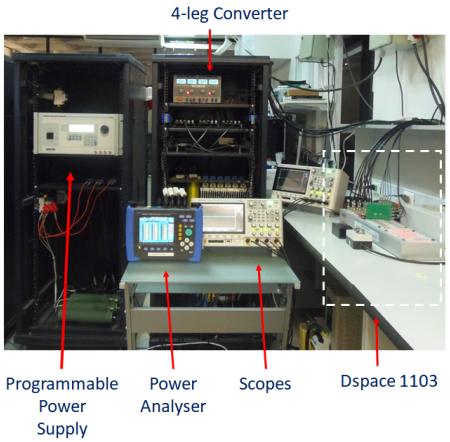

Fig. 6. Experimental system.

where $k_s \in [0, 1]$ is the scaling factor to maintain the same initial power factor. Hence, it is computed as

$$k_s = \frac{S_g^{ref} + \Delta S_g}{S_g^{ref}} \tag{46}$$

with $S_g^{ref} = ((P_g^{ref})^2 + (Q_g^{ref})^2)^{1/2}$.

It is worth to highlight that this approach is an indirect manner to limit the converter output currents.

IV. Simulation and Experimental Results

The control systems depicted in Fig. 2 have been implemented in the experimental system shown in Fig. 6. In this work, an Ametek 4-wire programmable power supply (model MX45), which is capable of generating programmable grid sag-swell conditions, emulates the ac-grid shown in Fig. 1. To experimentally validate the control strategies, a four-leg voltage source power converter, based on the Semikron SKM50GB123D IGBT module, was designed and built for this work. The control system shown in Fig. 6 is implemented using a DSPACE 1103 platform. Hall effect transducers are used to measure the voltages and currents required for the implementation of the control system depicted in Fig. 2. To synthesize the output voltages, a four-leg pulsewidth modulation (PWM) algorithm is implemented utilizing the off-the-shelf PWM modules available in the DSPACE 1103 control platform.

A. Results Without Using the Output Power Limiter

For the experimental results presented in this section, it is assumed that the overcurrent limiter introduced in section III-D is not required, and hence, it is not enabled. Hence, $k_S = 1$.

Fig. 7 shows the operation of the control methodology. In this case, the grid voltage is unbalanced with the amplitude of one-phase being reduced to 0.8 p.u.; the reference active power injected into the grid is 2 kW; the reference for the reactive power is 0 kVA; the parameter μ is set to 1. In Fig. 7(a), the waveforms of the converter-side and grid-side active powers, the reactive power injected into the grid, and also the dc-link current (scaled by one-fifth) are shown. On the other hand, Fig. 7(b) shows the grid currents. As depicted in this graph, before enabling the zero-sequence current injection, the three-phase currents are slightly unbalanced due to the negative-sequence current produced when the parameter $\mu = 1$. Hence, APOs at twice the utility frequency are present in both the converter- and grid-side active power; meanwhile, the reactive power is free of oscillations due to $\mu = 1$. Furthermore, when the zero-sequence reference generator is enabled, the rising of the neutral current increases the imbalance in the phase currents [see Fig. 7(b)], but it allows a complete elimination of the APO observed in the converter [see the orange line in Fig. 7(a)].

The harmonic spectrum of $p_s(t)$ for both operating modes is compared, as shown in Fig. 8. As it is shown, previous to the injection of the zero-sequence current, the amplitude

TABLE I
Parameters of the Experimental Setup

Parameter	Description	Value
f_s	Sampling frequency	10 kHz
f_g	Grid frequency	50 Hz
L_f	Inductive filter	5 mH
L_n	Neutral inductance	0.78 mH
R_f	Parasitic resistor	0.8Ω
C_{dc}	dc-link capacitance	9200μF
V_{dc}	dc-link voltage	450-500 V

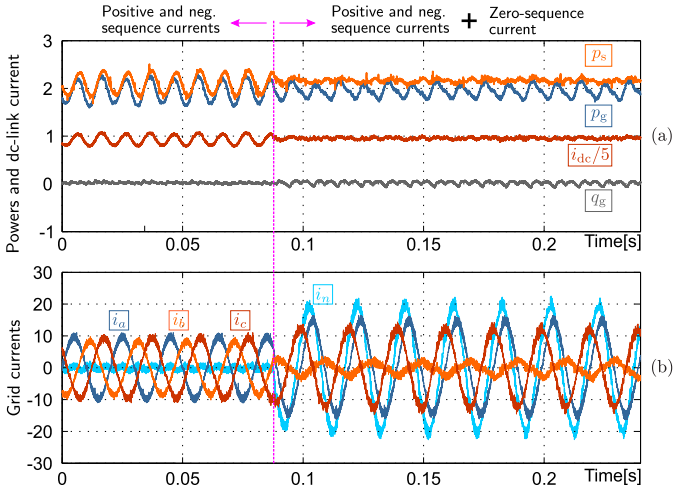

Fig. 7. Experimental results without using the OPL. Parameters: $\mu = 1$, $p_g^{ref} = 2$ [kW], $q_g^{ref} = 0$ [kVA], $V_{abc} = [0.8\ 1.0\ 1.0]^T$ in pu of 110 V_{rms}. (a) Active powers p_s, p_g[kW], reactive power q_g [kVA], and dc-link current i_{dc} [A/5]. (b) Grid currents [A].

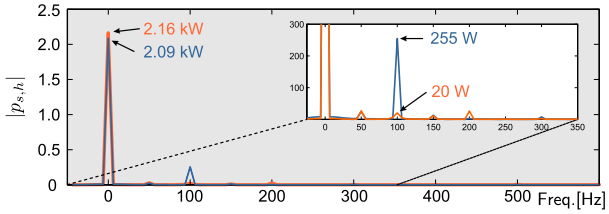

Fig. 8. Harmonic spectrum of converter active power p_s in Fig. 7(a).

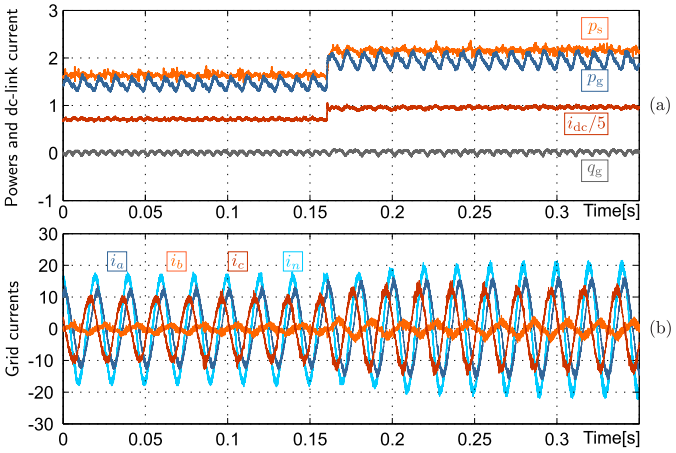

Fig. 9. Experimental result when a step-change in the active power reference is applied $p_{\rm g}^{\rm ref} = 1.5 \rightarrow 2.0$ [kW]. Parameters: $\mu = 1$, $q_g^{\rm ref} = 0$ [kVA], $V_{\rm abc} = [0.8\ 1.0\ 1.0]^T$ in pu of 110 $V_{\rm rms}$. (a) Active powers $p_{\rm s}$, $p_{\rm g}$ [kW], reactive power $q_{\rm g}$ [kVA], and dc-link current $i_{\rm dc}$ [A/5]. (b) Grid currents [A].

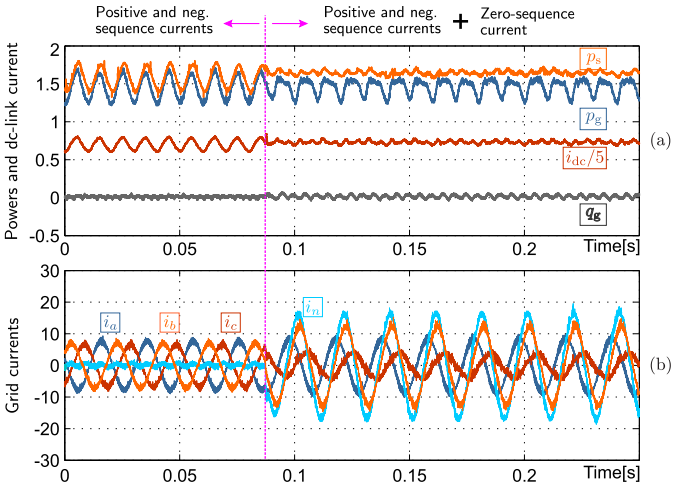

Fig. 10. Experimental results without using the OPL. Parameters: $\mu = 1$, $p_{\rm g}^{\rm ref} = 1.5$ [kW], $q_{\rm g}^{\rm ref} = 0$ [kVA], $V_{\rm abc} = [0.8\ 0.9\ 1.0]^T$ in pu of 110 $V_{\rm rms}$. (a) Active powers $p_{\rm s}$, $p_{\rm g}$[kW], reactive power $q_{\rm g}$ [kVA], and dc-link current $i_{\rm dc}$ [A/5]. (b) Grid currents [A].

of the 100-Hz component is 255 W (12.75% of the active power reference). However, after enabling the proposed control strategy [shown in Fig. 4], this oscillation decreases to 1%, which represents a relevant improvement. In addition, as the zero-sequence current also produces power losses in the equivalent resistance R_0, the dc-component of the active power delivered by the converter increases slightly by approximately 70 W (≈3.2%).

The dynamic performance of the proposed control system for step change variations is shown in Fig. 9. In this case, the reference for the active power $P_g^{\rm ref}$ is changed from 1.5 to 2.0 kW at instant $t \approx 0.16$ s with the proposed control algorithm enabled during the whole experimental test. The results are shown in Fig. 9, where it is concluded that the proposed control system is able to eliminate the APOs at the four-leg converter output even when the operating point of the system is subjected to a relatively large variation.

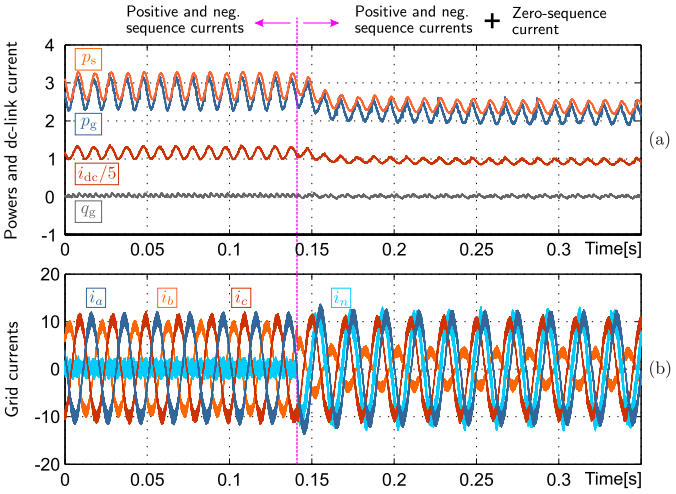

Fig. 11. Experimental results using the OPL. Parameters: $\mu = 1$, $p_{\rm g}^{\rm ref} = 2.75$ [kW], $q_{\rm g}^{\rm ref} = 0$ [kVA], $V_{\rm abc} = [0.8\ 1.0\ 1.0]^T$ in pu of 140 $V_{\rm rms}$. (a) Active powers $p_{\rm s}$, $p_{\rm g}$ [kW], reactive power $q_{\rm g}$ [kVA], and dc-link current $i_{\rm dc}$ [A/5]. (b) Grid currents [A].

As shown in Fig. 9(b), the PI-based regulator of the proposed zero-sequence signal has a good dynamic response to changes in the positive- and negative-sequence current components.

Finally, to show the flexibility of the proposed control strategy, a test similar to that shown in Fig. 7 is realized but using a higher degree of voltage imbalance ($V_{\rm abc} = [0.8\ 0.9\ 1.0]^T$ in p.u. of 110 $V_{\rm rms}$). The experimental results are depicted in Fig. 10. The active power reference to be injected into the grid is 1.5 kW, $Q_g^{\rm ref} = 0$ kVA. As shown in these experimental results, after the proposed control methodology is enabled, the active power delivered by the converter is free of oscillations at twice the fundamental frequency.

B. Results Considering Overcurrent Limiter

Fig. 11 shows the experimental results obtained with the OPL enabled. In this case, the active power reference is 2.75 kW. As shown in Fig. 11(b), before injecting the zero-sequence current, a negative-sequence current is injected to the grid due to the parameter $\mu = 1$. The zero-sequence current is zero because the proposed i_0-generator depicted in Fig. 4 has not been enabled yet. In $t \approx 0.14$ s, the zero-sequence current injection is enabled, and after the neutral current is regulated, the maximum amplitude of the converter currents is maintained inside the converter thermal limit, as shown in Fig. 11(b). Therefore, the proposed OPL [see Fig. 5] is operating correctly. As depicted in Fig. 11(a), due to the converter current limitation, the APO at the converter side has not been eliminated but only mitigated. Nevertheless, this can be overcome by setting $\mu = 0$.

Fig. 12 shows the performance of the same test shown in Fig. 11 but using $\mu = 0$. As depicted in Fig. 12(b), the grid currents before the injection of the neutral current are balanced because of the selection of the parameter μ [see (16)], and only the positive-sequence current is supplied by the power converter. In addition, according to (19) and (20), the amplitude of the APO at the PCC is reduced to half the

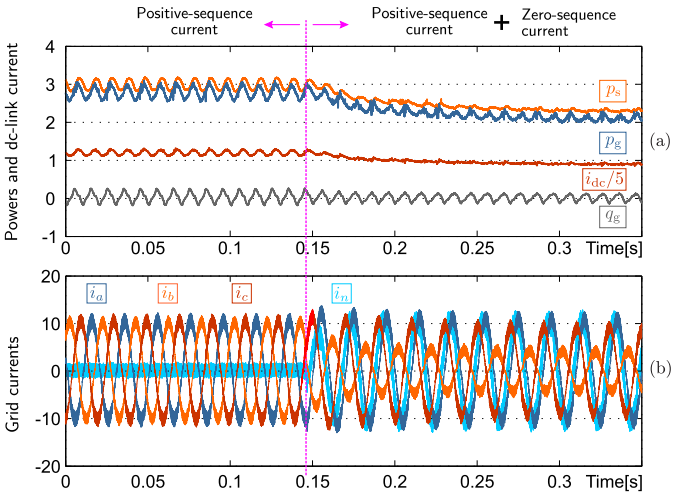

Fig. 12. Experimental results using the OPL Parameters: same as in Fig. 11, but $\mu = 0$. (a) Active powers p_s, p_g [kW], reactive power q_g [kVA], and dc-link current i_{dc} [A/5]. (b) Grid currents [A].

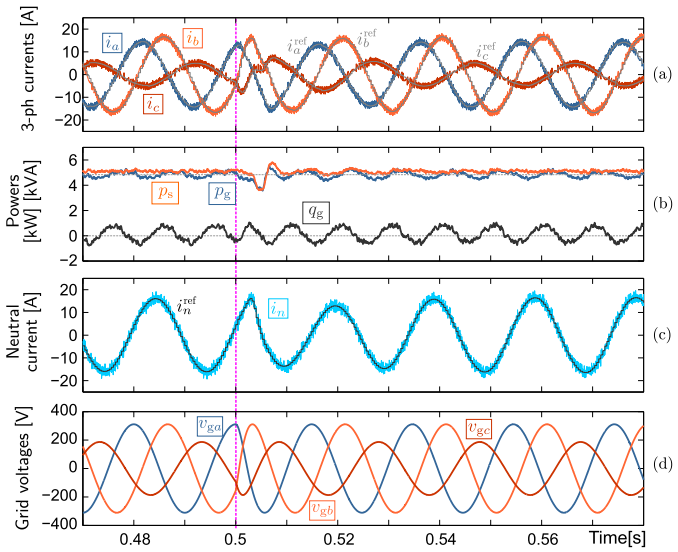

Fig. 13. Simulation result for a step-changed in the grid-frequency from 50 to 51 Hz considering noninjection of negative-sequence currents ($\mu = 0$) with $p_g^{ref} = 5$ [kW], $q_g^{ref} = 0$ [kVA], $V_{abc} = [1.0\ 1.0\ 0.6]^T$. (a) *abc* grid currents. (b) Active [kW] and reactive [kVA] powers. (c) Neutral current [A]. (d) Three-phase grid voltages [V].

value shown in the blue line in Fig. 5(b) (using $\mu = 1$). This experimental result confirms the aforementioned tradeoff between the amplitude of the active/reactive oscillations when the parameter μ is tuned. Finally, in $t \approx 0.14$ s, the proposed APO elimination methodology is enabled, and the active power supplied by the converter is free of double-frequency components when a zero-sequence current is injected into the system. In this case, positive- and zero-sequence currents are flowing into the *abc* phases of the converter, as depicted in Fig. 12(b).

C. Simulation Results

In this section, the simulation work is realized in order to study the influence of (25) in the dynamic performance of the proposed control algorithm and to study the robustness of the system to a 2% variation in the grid frequency. The performance of the control system to a 2% variation in the grid frequency is shown in Fig. 13. Initially, the system is operating with an unbalanced voltage in phase *c* of 130-V rms (the other two phases are operating at the nominal voltage of 220-V rms). The total load is about 5-kW grid side [see the blue line p_g in Fig. 13(b)] with the proposed control system, eliminating APOs at the converter side [see the red line p_s in Fig. 13(b)]. The neutral current is limited to the rated value [see Fig. 13(c)] because the overcurrent limiter depicted in Fig. 5 is being enabled. In addition, the converter is not injecting negative-sequence currents because the parameter μ is adjusted to 0 for this test [see (16)]. Consequently, RPOs at the grid side emerge as a results of the interaction of the positive-sequence current and the negative-sequence voltage, as shown in (20).

At instant $t = 0.2$, the frequency is step-changed from 50 to 51 Hz. The perturbation is controlled with a settling time of ≈14 ms (i.e., slightly higher to half a cycle), and this is a broad agreement with the results obtained from (25), which predict a maximum settling time of about 15 ms for the dynamic performance of the APF. Note that after the perturbation produced in $t = 0.2$ s, the voltage, current, and power waveforms are stable and operating without any noticeable distortion. In the steady state, the APOs are effectively eliminated at the converter side.

On the other hand, the performance in the control system for a step variation in the voltage of phase c (grid side) is shown in Fig. 14. Initially, the system is operating with balanced voltages and currents [see Fig. 14(a) and (e)], injecting 7.5 kW at the grid side with the reactive power reference set to $q_g = 0$ kVA [see Fig. 14(b)]. In $t = 0.2$ s, the magnitude of the grid voltage in phase *c* is step-changed and to 130-V rms, as shown in Fig. 14(b), oscillating power components of 100 Hz are produced in the active/reactive powers at the grid and converter sides. For this test, the parameter μ is also adjusted to zero to avoid injecting the negative-sequence current.

In Fig. 14(d), the oscillating components of the active power are shown referred to a dq-coordinate axis rotating at twice the grid frequency. After $t = 0.2$ s, oscillations in the active power are produced as a consequence of the unbalanced voltages (and this is reflected in the dq components), reaching a peak value of about 600 W. The proposed control system shown in Fig. 2 is used to eliminate the APOs with a settling time of about 0.15–0.2 s maintaining all the currents within their rated limit.

Note that the settling time of 0.15 s is about ten times the settling time of the APF [see (25)]. Therefore, a good decoupling between the dynamic of the implemented APF with notch and band filters, and the dynamic of the zero-sequence generator control loop is achieved in the overall control system.

The APO scheme is not designed for a very fast dynamic because this is not the sort of application being studied in this work. The settling time of the control system, shown in Fig. 14(d), is enough to maintain the voltage oscillation controlled when the relatively low-frequency variations in the imbalance of the grid are considered.

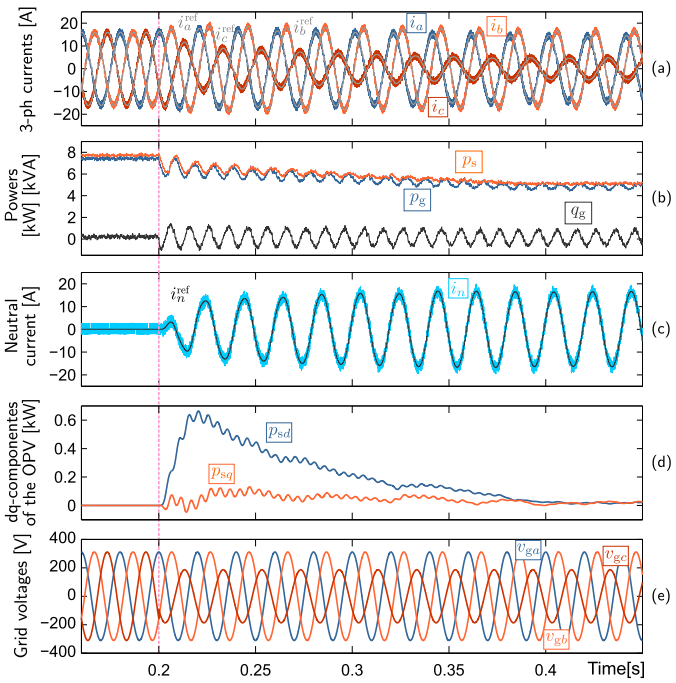

Fig. 14. Simulation result for step decreasing voltage considering non-injection of negative-sequence currents ($\mu = 0$) with an initial condition $p_g^{\text{ref}} = 7.5$ kW, $q_g^{\text{ref}} = 0$ kVA, $V_{\text{abc}} = [1.0\ \ 1.0\ \ 1.0 \rightarrow 0.6]^T$. (a) *abc* grid currents [A]. (b) Active [kW] and reactive [kVA] powers. (c) Neutral current [A]. (d) Converter side oscillating active power in *dq* coordinates. (e) Three-phase grid voltages [V].

Note that, in Figs. 13(a) and 14(a), the reference signals for the currents are included. By inspecting the graphics, it is concluded that zero-steady-state error is achieved with the proposed control methodology.

V. Conclusion

This paper presents a novel methodology to eliminate power oscillations in four-leg power converters connected to unbalanced networks. To achieve this target, the zero-sequence power delivered by the converter is used to eliminate the power oscillations produced by the positive- and negative-sequence components of the grid voltages and currents. This control strategy is based on a vector representation of the oscillating active power, which allows a simple and efficient implementation of a PI controller in an SRF rotating at twice the grid frequency. The proposed control strategy is implemented with an innovate current limiter that reduces the active/reactive power references maintaining the power factor to avoid operations outside the thermal limit of the converter. In addition, the proposed strategy provides an extra degree of freedom, given by the parameter μ, which enables eliminating the oscillating active power even when the amplitude of the zero-sequence current is limited to its rated value.

The effectiveness of the proposed control strategy has been proven by experimental results considering several steady-state operating conditions, different degrees of grid voltage imbalances, and sudden step changes in the power references. In all the cases, the results obtained were excellent.

References

[1] J. M. Guerrero, L. Hang, and J. Uceda, "Control of distributed uninterruptible power supply systems," *IEEE Trans. Ind. Electron.*, vol. 55, no. 8, pp. 2845–2859, Aug. 2008.

[2] D. E. Olivares *et al.*, "Trends in microgrid control," *IEEE Trans. Smart Grid*, vol. 5, no. 4, pp. 1905–1919, Jul. 2014.

[3] S. K. Sahoo, A. K. Sinha, and N. K. Kishore, "Control techniques in AC, DC, and hybrid AC–DC microgrid: A review," *IEEE J. Emerg. Sel. Topics Power Electron.*, vol. 6, no. 2, pp. 738–759, Jun. 2018.

[4] T. Gonen, *Electric Power Distribution Engineering*, 3rd ed. Boca Raton, FL, USA: CRC Press, 2014, p. 1036.

[5] M. Z. Kamh and R. Iravani, "Unbalanced model and power-flow analysis of microgrids and active distribution systems," *IEEE Trans. Power Del.*, vol. 25, no. 4, pp. 2851–2858, Oct. 2010.

[6] R. Cárdenas, C. Juri, R. Peña, P. Wheeler, and J. Clare, "The application of resonant controllers to four-leg matrix converters feeding unbalanced or nonlinear loads," *IEEE Trans. Power Electron.*, vol. 27, no. 3, pp. 1120–1129, Mar. 2012.

[7] F. Rojas, R. Cárdenas, R. Kennel, J. C. Clare, and M. Diaz, "A simplified space-vector modulation algorithm for four-leg NPC converters," *IEEE Trans. Power Electron.*, vol. 32, no. 11, pp. 8371–8380, Nov. 2017.

[8] C. Burgos-Mellado, R. Cárdenas, D. Sáez, A. Costabeber, and M. Sumner, "A control algorithm based on the conservative power theory for cooperative sharing of imbalances in four-wire systems," *IEEE Trans. Power Electron.*, vol. 34, no. 6, pp. 5325–5339, Jun. 2019.

[9] S. Beheshtaein, M. Savaghebi, R. Cuzner, S. Golestan, and J. M. Guerrero, "A modified secondary-control based fault current limiter for four-wire three phase DGS," *IEEE Trans. Ind. Electron.*, to be published.

[10] I. Sadeghkhani, M. E. H. Golshan, A. Mehrizi-Sani, and J. M. Guerrero, "Low-voltage ride-through of a droop-based three-phase four-wire grid-connected microgrid," *IET Gener. Transm. Distrib.*, vol. 12, no. 8, pp. 1906–1914, Apr. 2018.

[11] C. Burgos-Mellado *et al.*, "Experimental evaluation of a CPT-based four-leg active power compensator for distributed generation," *IEEE J. Emerg. Sel. Topics Power Electron.*, vol. 5, no. 2, pp. 747–759, Jun. 2017.

[12] Q. Tabart, I. Vechiu, A. Etxeberria, and S. Bacha, "Hybrid energy storage system microgrids integration for power quality improvement using four-leg three-level NPC inverter and second-order sliding mode control," *IEEE Trans. Ind. Electron.*, vol. 65, no. 1, pp. 424–435, Jan. 2018.

[13] K. Ma, W. Chen, M. Liserre, and F. Blaabjerg, "Power controllability of a three-phase converter with an unbalanced AC source," *IEEE Trans. Power Electron.*, vol. 30, no. 3, pp. 1591–1604, Mar. 2015.

[14] A. J. Roscoe, S. J. Finney, and G. M. Butt, "Tradeoffs between AC power quality and DC bus ripple for 3-phase 3-wire inverter-connected devices within microgrids," *IEEE Trans. Power Electron.*, vol. 26, no. 3, pp. 674–688, Mar. 2011.

[15] S. Roediger, R. Yan, and T. K. Saha, "Investigation of the impacts of three-phase photovoltaic systems on three-phase unbalanced networks," in *Proc. IEEE Power Energy Soc. Gen. Meeting*, Jul. 2012, pp. 1–8.

[16] L. Fan, Z. Miao, and A. Domijan, "Impact of unbalanced grid conditions on PV systems," in *Proc. IEEE PES Gen. Meeting*, Jul. 2010, pp. 1–6.

[17] Q.-C. Zhong, W.-L. Ming, X. Cao, and M. Krstic, "Control of ripple eliminators to improve the power quality of DC systems and reduce the usage of electrolytic capacitors," *IEEE Access*, vol. 4, pp. 2177–2187, May 2016.

[18] F. Wang, J. L. Duarte, and M. A. M. Hendrix, "Pliant active and reactive power control for grid-interactive converters under unbalanced voltage dips," *IEEE Trans. Power Electron.*, vol. 26, no. 5, pp. 1511–1521, May 2011.

[19] R. Teodorescu, M. Liserre, and P. Rodriguez, *Grid Converters for Photovoltaic and Wind Power Systems*. Hoboken, NJ, USA: Wiley, 2011.

[20] R. Cárdenas, M. Díaz, F. Rojas, J. Clare, and P. Wheeler, "Resonant control system for low-voltage ride-through in wind energy conversion systems," *IET Power Electron.*, vol. 9, no. 6, pp. 1297–1305, May 2016.

[21] S. Alepuz *et al.*, "Control strategies based on symmetrical components for grid-connected converters under voltage dips," *IEEE Trans. Ind. Electron.*, vol. 56, no. 6, pp. 2162–2173, Jun. 2009.

[22] R. Kabiri, D. G. Holmes, and B. P. McGrath, "Control of active and reactive power ripple to mitigate unbalanced grid voltages," *IEEE Trans. Ind. Appl.*, vol. 52, no. 2, pp. 1660–1668, Mar./Apr. 2016.

[23] A. Camacho, M. Castilla, J. Miret, A. Borrell, and L. G. de Vicuña, "Active and reactive power strategies with peak current limitation for distributed generation inverters during unbalanced grid faults," *IEEE Trans. Ind. Electron.*, vol. 62, no. 3, pp. 1515–1525, Mar. 2015.

[24] P. Rodriguez, A. Luna, J. Hermoso, I. Etxeberria-Otadui, R. Teodorescu, and F. Blaabjerg, "Current control method for distributed generation power generation plants under grid fault conditions," in *Proc. IEEE 37th Annu. Conf. Ind. Electron. Soc. (IECON)*, Nov. 2011, pp. 1262–1269.
[25] M. Castilla, J. Miret, J. L. Sosa, J. Matas, and L. G. de Vicuña, "Grid-fault control scheme for three-phase photovoltaic inverters with adjustable power quality characteristics," *IEEE Trans. Power Electron.*, vol. 25, no. 12, pp. 2930–2940, Dec. 2010.
[26] A. Mora, R. Cárdenas, M. Espinoza, and M. Díaz, "Active power oscillation elimination in 4-leg grid-connected converters under unbalanced network conditions," in *Proc. 42nd Annu. Conf. IEEE Ind. Electron. Soc. (IECON)*, Oct. 2016, pp. 2229–2234.
[27] H. Akagi, E. H. Watanabe, and M. Aredes, *Instantaneous Power Theory and Applications to Power Conditioning*. Hoboken, NJ, USA: Wiley, 2017.
[28] P. M. Anderson, *Analysis of Faulted Power Systems*. Piscataway, NJ, USA: IEEE Press, 1995.
[29] G. C. Paap, "Symmetrical components in the time domain and their application to power network calculations," *IEEE Trans. Power Syst.*, vol. 15, no. 2, pp. 522–528, May 2000.
[30] P. Rodriguez, A. V. Timbus, R. Teodorescu, M. Liserre, and F. Blaabjerg, "Flexible active power control of distributed power generation systems during grid faults," *IEEE Trans. Ind. Electron.*, vol. 54, no. 5, pp. 2583–2592, Oct. 2007.
[31] J. Eloy-García, S. Arnaltes, and J. L. Rodríguez-Amenedo, "Direct power control of voltage source inverters with unbalanced grid voltages," *IET Power Electron.*, vol. 1, no. 3, pp. 395–407, Sep. 2008.
[32] Y. F. Wang and Y. W. Li, "Grid synchronization PLL based on cascaded delayed signal cancellation," *IEEE Trans. Power Electron.*, vol. 26, no. 7, pp. 1987–1997, Jul. 2011.
[33] R. Cárdenas, M. Díaz, F. Rojas, and J. Clare, "Fast convergence delayed signal cancellation method for sequence component separation," *IEEE Trans. Power Del.*, vol. 30, no. 4, pp. 2055–2057, Aug. 2015.
[34] M. Monfared, S. Golestan, and J. M. Guerrero, "Analysis, design, and experimental verification of a synchronous reference frame voltage control for single-phase inverters," *IEEE Trans. Ind. Electron.*, vol. 61, no. 1, pp. 258–269, Jan. 2014.

Andrés Mora (M'17) was born in Santiago, Chile. He received the B.Sc. and M.Sc degrees in electrical engineering from Universidad Técnica Federico Santa María (UTFSM), Valparaíso, Chile, in 2010, and the Ph.D. degree in electrical engineering from the Universidad de Chile, Santiago, Chile, in 2019.

Since 2011, he has been an Assistant Professor with the Department of Electrical Engineering, UTFSM. His current research interests include multilevel power converters, variable speed drives, model predictive control, and renewable energy conversion systems.

Roberto Cárdenas (SM'07) was born in Punta Arenas, Chile. He received the B.S. degree from the University of Magallanes, Punta Arenas, in 1988, and the M.Sc. and Ph.D. degrees from the University of Nottingham, Nottingham, U.K., in 1992 and 1996, respectively.

From 1989 to 1991 and 1996 to 2008, he was a Lecturer with the University of Magallanes. From 1991 to 1996, he was with the Power Electronics Machines and Control Group (PEMC Group), University of Nottingham. From 2009 to 2011, he was with the Electrical Engineering Department, University of Santiago. He is currently a Professor in power electronics and drives with the Electrical Engineering Department, University of Chile, Santiago, Chile.

Dr. Cárdenas is a Senior Member of the Institute of Electrical and Electronic Engineers. He was a recipient of the Best Paper Award from the IEEE TRANSACTIONS ON INDUSTRIAL ELECTRONICS in 2005. His current interests include control of electrical machines, variable speed drives. and renewable energy systems.

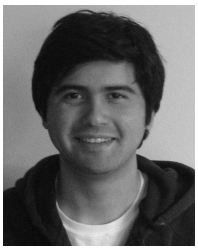

Matías Urrutia (S'17) was born in Santiago, Chile, in 1991. He received the degree in engineering and the M.Sc. degree in electrical engineering from Universidad Técnica Federico Santa María (UTFSM), Valparaíso, Chile, in 2017. He is currently pursuing the Ph.D. degree in electrical engineering with the University of Chile, Santiago.

His current research interests include modular multilevel converters control and FPGA-based digital control schemes for power electronics applications.

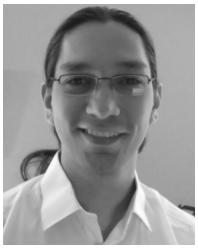

Mauricio Espinoza (M'19) was born in Alajuela, Costa Rica. He received the B.S. and Lic. degrees in electrical engineering from the University of Costa Rica, San Pedro, Costa Rica, in 2010 and 2012, respectively, and the Ph.D. degree in electrical engineering from the University of Chile, Santiago, Chile, in 2018.

From 2010 to 2019, he was a Lecturer with the University of Costa Rica. During his career, he was involved in research projects related to modular multilevel converters, machine modeling, and control systems for power electronics.

Matías Díaz was born in Santiago, Chile. He received the B.Sc. and M.Sc. degrees in electrical engineering from the University of Santiago of Chile, Chile, in 2011, the dual Ph.D. degrees from the University of Nottingham, Nottingham, U.K., and the University of Chile, Santiago, Chile.

He is currently an Assistant Professor with the University of Santiago of Chile. His current research interests include the control of wind energy conversion systems and multilevel converters.